

When are galactic winds molecular?

Aditi Vijayan^{1,2*} and Mark R. Krumholz^{1,2}

¹Research School of Astronomy and Astrophysics, Australian National University, Cotter Road, Weston ACT 2612, Australia

²ARC Centre of Excellence for Astronomy in Three Dimensions (ASTRO-3D), Canberra ACT 2601, Australia

Accepted XXX. Received YYY; in original form ZZZ

ABSTRACT

The molecular phase of supernova-driven outflows originates from the cold, molecular gas in the disc of a star-forming galaxy, and may carry a substantial fraction of the wind mass flux in some galaxies, but it remains poorly understood. Observations of this phase come mostly from very nearby galaxies due its low surface brightness and covering fraction, and simulations often lack the spatial resolution necessary to resolve it. Here we analytically estimate the survivability of this phase in order to understand under what conditions an galactic wind can contain a significant molecular phase. We show that the molecular content of outflows is primarily determined by two dimensionless numbers: a generalised Eddington ratio describing the strength of the outflow and an ionisation parameter-like quantity describing the strength of the radiation field per baryon. We apply this model to a sample of galaxies and show that, while any molecules entrained in the winds of normal star-forming galaxies should be destroyed close to the galactic disc, the outflows of strong starburst should become increasingly dominated by molecules.

Key words: astrochemistry – galaxies: ISM – galaxies: starburst – ISM: outflows – ISM: molecules

1 INTRODUCTION

In star-forming galaxies, supernova-driven multiphase, panchromatic outflows act as a conduit for mass, momentum, energy and metal exchange between a galaxy and its surrounding gas. Theoretical work suggests that different phases of the outflows are responsible for carrying different parts of this flow, with hot gas dominating the energy and metal flux while cooler gas dominates the mass flux (e.g., Li & Bryan 2020; Kim et al. 2020a,b; Schneider et al. 2020; Rathjen et al. 2021; Vijayan et al. 2024). This suggests that understanding the cool phase of the outflows is key for understanding the broader baryon cycle as well as the regulation of star formation within galaxies. However, “cool” gas – usually denoting gas at temperatures $\lesssim 10^4$ K – is not a single phase. Instead, it can be further subdivided into a phase at $T \sim 10^4$ K where the hydrogen is mostly ionised, a neutral hydrogen phase with temperatures $T \sim 200\text{--}7000$ K, and a molecular phase where most hydrogen is locked into H_2 molecules and the gas temperature falls to $T \sim 10\text{--}100$ K. In galaxies with star formation rates high enough to drive substantial outflows, particularly beyond $z = 0$, the molecular phase usually dominates the mass budget of the interstellar medium (Tacconi et al. 2020), but it is unclear to what extent this translates to the mass budget of the outflows.

The question of how cool outflows further subdivide into ionised, neutral, and molecular components has proven difficult to study in numerical simulations due to resolution. Even the transition between the $T \sim 10^6$ K and $T \sim 10^4$ K ionised phases is challenging to capture properly in simulations because it depends on processes such as Kelvin-Helmholtz and Rayleigh-Taylor instabilities in turbulent boundary layers that are seldom to never resolved in galaxy-scale simulations (e.g., Fielding & Bryan 2022, and references therein).

The neutral and molecular phases, which are typically much denser than the $\sim 10^4$ K ionised phase, are even harder to resolve, and consequently many simulations do not even attempt to include the cooling or chemical processes relevant to them (though there are exceptions, e.g., Kim et al. 2020b; Rathjen et al. 2021; Chen & Oh 2023; Vijayan et al. 2024). Similarly, semi-analytic models for multiphase outflows (Huang et al. 2020, 2022; Weinberger & Hernquist 2023; Smith et al. 2024; Butsky et al. 2024), which are calibrated from these simulations, generally ignore the distinction between molecular, atomic, and cool ionised gas, instead lumping them into a single “cool” phase.

The phase structure of the cool gas has also proven difficult to study observationally. While the ionised component is seen ubiquitously in both absorption and emission studies (Veilleux et al. 2020, and references therein), the atomic and molecular phases are much more challenging to study because their small filling factor makes them difficult to see in absorption, and their low surface brightness makes them difficult to see in emission. To date there have been only a few detections of these components of outflows from star-forming galaxies reported in literature. Perhaps the best-studied example is M82, where both atomic (Martini et al. 2018) and molecular (Leroy et al. 2015) gas have been mapped from the base of the outflow where it joins the ISM up to distances of \sim few kpc above the disc. Quantitative analysis of these data indicates that the atomic and molecular phases likely carry as much or more mass flux than the cool ionised phase (Yuan et al. 2023). Other local examples of molecular outflows include NGC 253 (Bolatto et al. 2013; Walter et al. 2017) and the Large Magellanic Cloud (Tchernyshyov 2022), and there is indirect evidence from stacks of high redshift galaxies that many also possess large molecular outflows (Ginolfi et al. 2017). Finally, in the central region of the Milky Way, Di Teodoro et al. (2018, 2020) detect a large population of outflowing clouds containing a mix of neutral and molecular hydrogen. Noon et al. (2023) show that these clouds

* E-mail: aditi.vijayan@anu.edu.au (AV)

are predominantly molecular close to the Galactic plane but become increasingly atomic at large distances, and that they are characterised by a disequilibrium chemical state suggesting that the molecules are in the process of photodissociating as the clouds move away from the Galaxy.

Given the difficulty of studying in particular the atomic and molecular parts of outflows from both simulations and observations, it is helpful to turn to analytic models that can be used as a guide for future work. That is our goal here: in this work, we present a predictive theoretical model for quantifying the molecular fraction in a galactic outflow, focusing in particular on the balance between the neutral and ionised phases, the two that are least-studied by both observations and theory. We explore the parameter space of galaxy masses, star formation rates, and dynamical times and understand which of these are important for a galaxy to host molecular outflows. Our ultimate goal is a first-order answer to the basic question: for which galaxies is it likely that a substantial component of the mass flux will be carried by the molecular phase of the outflow? The layout of the paper is as follows. [Section 2](#) we introduce the model and its assumptions. In [Section 3](#) we apply the model to make predictions about the molecular content of outflows as a function of galaxy properties, and apply those predictions to observed galaxies. We conclude and discuss future prospects in [Section 4](#).

2 THE MODEL

Here we provide a model to understand the atomic-molecular balance in outflows, and in particular to understand under what circumstances we expect the non-ionised part of the outflow to contain a substantial molecular component, versus when we expect it to be fully atomic. We begin in [Section 2.1](#) with a general discussion of radiative versus collisional processes, and then in [Section 2.2](#) we use this discussion to develop a simple but predictive model for the atomic-to-molecular ratio in single cloud, which we extend to the full wind in [Section 2.3](#).

2.1 Radiative versus collisional processes

As noted in [Section 1](#), the bulk of the mass available to be launched into outflows in most galaxies with substantial star formation rates exists in molecular form in the disc, and spatially resolved observations in both the Milky Way centre and M82 indicate that near their launch point most of the mass in outflows is molecular, with the balance shifting toward atomic further from the galaxy. However, free atomic hydrogen is a higher energy state than hydrogen molecules, and in the absence of a dissociative process a cloud of free atomic hydrogen will spontaneously convert to H_2 on timescales of Myr. Thus if an outflow contains significant amounts of atomic hydrogen, there must be some mechanism that dissociates H_2 molecules and inhibits this conversion. This mechanism could be either collisional – for example, mixing of supernova-heated gas into the outflow which keeps it warm enough to dissociate H_2 – or radiative, in the form of Lyman-Werner band photons that excite the H_2 molecules into the $B^1\Sigma_u$ or $C^1\Pi_u$ electronic states, from which they can de-excite into the unbound continuum of the ground $X^1\Sigma_g^+$ electronic state. Our first task in constructing a model for molecular outflow is to determine which of these channels is likely to be dominant.

To answer this question we can compare collisional and radiative dissociation rates. In a predominantly atomic medium the main collisional dissociation channel is

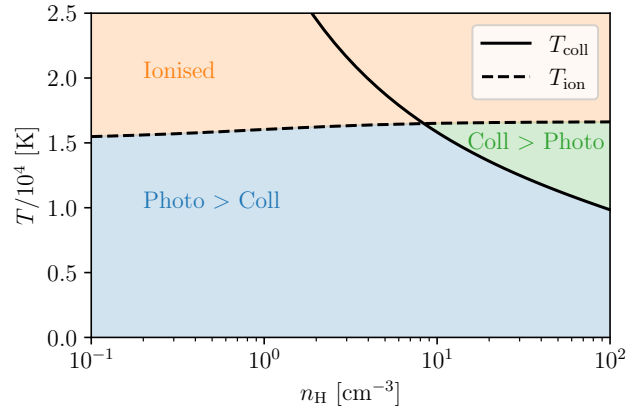


Figure 1. The temperatures T_{coll} at which collisional dissociation becomes more important than photodissociation (solid line), and T_{ion} at which hydrogen is 50% collisionally ionised (dashed line), as a function of number density of H nuclei n_{H} . These lines divide the plane into three regions: one where photodissociation is the dominant producer of atomic hydrogen (blue), one where collisional dissociation dominates (green), and one where no neutral gas is present due to collisional ionisation (orange). We see that collisional dissociation can only ever be dominant at densities $n_{\text{H}} \gtrsim 10 \text{ cm}^{-3}$, and then only over a narrow range of temperatures from $\approx 1.0 - 1.6 \times 10^4$ K.

so the collisional dissociation rate per unit time per H_2 molecule is $k_{\text{H}}n_{\text{H}}$; we take our rate coefficient k_{H} as a function of n_{H} and gas temperature T from equation 26 of [Glover & Mac Low \(2007\)](#), and note that, as expected, k_{H} is a monotonically increasing function of T . The competing photodissociation channel occurs at a rate that depends on the intensity of the radiation field. The [Draine \(1978\)](#) field that is typical of the Milky Way near the Solar neighbourhood produces a dissociation rate $D_0 = 5.8 \times 10^{-11} \text{ s}^{-1}$ ([Sternberg et al. 2014](#)), so we take the photodissociation rate to be χD_0 , with $\chi = 1$ corresponding to the [Draine](#) field. Thus the condition $n_{\text{H}}k_{\text{H}} = \chi D_0$ implicitly specifies a minimum temperature T_{coll} above which the collisional channel dominates and below which the radiative channel does.

However, the temperature cannot be arbitrarily high if H I is to be present – if T is too large, then the gas will collisionally ionise and become dominated by H^+ instead. We define T_{ion} as the temperature below which gas in collisional ionisation equilibrium will have $< 50\%$ of its hydrogen ionised. We compute T_{ion} as a function of n_{H} using the astrochemistry code `DESPTIC` ([Krumholz 2014](#)), using the [Gong et al. \(2017\)](#) chemical network with an ambient non-ionising radiation field $\chi = 1$, zero ionising radiation, and a cosmic ray ionisation rate of $2 \times 10^{-16} \text{ s}^{-1}$ ([Indriolo & McCall 2012](#)). We see that the hydrogen reaches 50% collisional ionisation at $T \approx 1.6 \times 10^4$ K, with only an extremely weak dependence on density.

Thus the condition for dissociation to be dominant over photoionisation reduces to the requirement that $T_{\text{coll}} < T < T_{\text{ion}}$. We plot T_{coll} and T_{ion} as a function of n_{H} , for $\chi = 1$, in [Figure 1](#). The plot shows that collisional dissociation is never more important than photodissociation at densities $\lesssim 10 \text{ cm}^{-3}$, and that at higher densities collisional dissociation dominates only over a fairly narrow range in temperature, from $\approx 1.0 - 1.6 \times 10^4$ K. Our conclusion based on this is that photodissociation will be dominant in most circumstances, and we will therefore proceed to build our model for the chemical state of outflows focusing on this process.

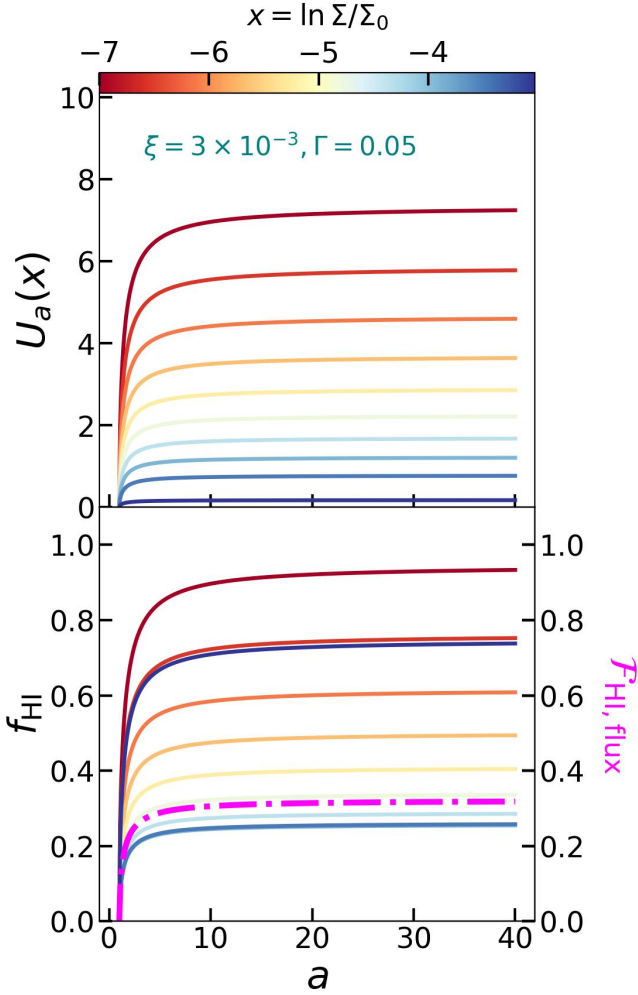


Figure 2. The acceleration law (top), H I fraction f_{HI} (bottom, solid curves), and flux-averaged H I fraction $F_{\text{HI, flux}}$ (bottom, dot-dashed magenta line), for a wind with clouds of fixed area driven by a galaxy with a point source potential; different coloured solid lines indicate different values of the dimensionless cloud surface density x , as indicated in the colour bar. The example shown uses the parameters $\xi = 3 \times 10^{-3}$, $\Gamma = 0.05$, and $M = 1000$.

2.2 The atomic-to-molecular transition in a single cloud

Now that we have determined that our focus should be on radiative rather than collisional processes, we build a model to determine when radiation is expected to yield outflow with a high molecular content, versus when it is expected to efficiently dissociate most H_2 molecules, which we build on top of the model for momentum-driven cool winds proposed by Krumholz et al. (2017), building on earlier work by Thompson & Krumholz (2016), to which we refer hereafter as the *KTOM* model. This model has been validated by comparison to both full 3D simulations (Raskutti et al. 2017) and observations of the wind of M82 (Yuan et al. 2023). In this model, clouds are continuously launched at a radius r_0 from a star-forming disc with mean surface density $\bar{\Sigma}_0$. The clouds in the disk possess a log-normal distribution of surface densities. A cloud will be launched into the wind if its surface density, Σ , satisfies $x = \ln \Sigma / \bar{\Sigma}_0 < x_{\text{crit}} = \ln \Gamma$, where Γ is the generalised Eddington ratio, quantifying the competition between gravity and momentum injection – $\Gamma = 1$ corresponds

to a galaxy where feedback and gravitational forces are equal for a cloud with surface density $\bar{\Sigma}_0$.

Once launched, a cloud moves radially outward, following a trajectory whereby its velocity at any given radius can be written $v(r) = v_0 U_a(x)$, where $v_0 = \sqrt{2GM_0/r_0}$ is the escape speed from r_0 , M_0 is the gravitating mass interior to r_0 , and $a = r/r_0$ is a dimensionless radius. The function $U_a(x)$ is called the wind acceleration law, and in the idealised case of a wind driving mechanism that simply supplies momentum at a fixed rate per unit area – the only case we will consider here – depends on the initial dimensionless cloud surface density x , on the generalised Eddington factor for the wind Γ , on the shape of the gravitational potential (e.g., point mass-like versus isothermal), and on the rate at which clouds’ cross-sectional areas expand as they travel outward in the wind. We refer readers for *KTOM* for a discussion of how $U_a(x)$ is calculated, and for the remainder of this paper simply adopt their results.

2.2.1 Fixed Area Case

We first consider the simplest case of clouds that maintain a fixed cross-sectional area as they travel outward. For a point-like gravitational potential, these clouds obey an acceleration law,

$$U_a^2(x) = (\Gamma e^{-x} - 1) \left(\frac{a-1}{a} \right). \quad (2)$$

For the purpose of illustration, in the top panel of Figure 2 we plot $U_a(x)$ as a function of a for a few different values of x . For this fixed-area, point-potential case, the clouds accelerate rapidly up to $a \lesssim 5$ and then move with a constant speed.

Now let us consider a cloud that is entirely molecular at the time when it enters the wind, consistent with observations showing that outflows are largely molecular at their base, and estimate how quickly it will be converted to a purely atomic one. As we have seen the dominant process will be photodissociation, and a radiation field of normalised strength χ provides a dissociating photon flux $F^* = 2 \times 10^7 \chi$ photons $\text{cm}^2 \text{s}^{-1}$ on the surface of a molecular cloud (Krumholz et al. 2009). For small cloud column densities ($\lesssim 10 M_\odot \text{pc}^{-2}$ at Solar metallicity, and thus applicable to most clouds with column densities small enough to be picked up by the wind), this radiation field will result in an H_2 dissociation rate that greatly exceeds the formation rate, so the mass per unit time per unit area dissociated from molecular to atomic composition will be $\dot{\Sigma}_{\text{diss}} = 2m_{\text{H}} f_{\text{diss}} F^* \equiv \chi \dot{\Sigma}_{\text{diss},0}$, where $\dot{\Sigma}_{\text{diss},0} = 1.5 M_\odot \text{pc}^{-2} \text{Myr}^{-1}$ is the dissociation rate expected for $\chi = 1$, and $f_{\text{diss}} \approx 0.15$ is the fraction of photon absorptions that result in a dissociation rather than radiative de-excitation back to a bound molecular state (Noon et al. 2023). We let χ_0 be the radiation field intensity at r_0 , and assume that the radiation field is dominated by the central galaxy, and therefore falls off as $\chi \propto 1/r^2$. With this assumption, we can write the rate of change in atomic hydrogen surface density as $\dot{\Sigma}_{\text{HI}} = \chi_0 \dot{\Sigma}_{\text{diss},0} / a^2$, and the rate of change with respect to radius is therefore

$$\frac{d\Sigma_{\text{HI}}}{da} = \frac{\chi_0 t_0 \dot{\Sigma}_{\text{diss},0}}{a^2 U_a(x)}, \quad (3)$$

for $\Sigma_{\text{HI}} < \Sigma$; here we have defined $t_0 = r_0/v_0$.

We are interested in tracking the atomic mass fraction, $f_{\text{HI}} = \Sigma_{\text{HI}} / \bar{\Sigma}_0 e^x$, as a function of distance a . We can express this as

$$\frac{df_{\text{HI}}}{da} = \frac{\chi_0 \dot{\Sigma}_{\text{diss},0} t_0}{\bar{\Sigma}_0 e^x} \frac{1}{a^2 U_a(x)}, \quad (4)$$

for $f_{\text{HI}} < 1$. The above equation has an exact solution with the

boundary condition $f_{\text{HI}}(a = 1) = 0$,

$$f_{\text{HI}} = \min \left(\frac{2\chi_0 \dot{\Sigma}_{\text{diss},0} t_0 e^{-x}}{\bar{\Sigma}_0 \sqrt{\Gamma e^{-x} - 1}} \sqrt{\frac{a-1}{a}}, 1 \right). \quad (5)$$

We plot f_{HI} as a function of a in the middle panel of [Figure 2](#) for a range of x values and using the sample parameters $\Gamma = 0.05$ and $\xi = 3 \times 10^{-3}$. As with $U_a(x)$, we see that f_{HI} attains a steady value at $a \gtrsim 5$. Clouds with larger surface density at the beginning of their trajectory reach atomic fractions of $\approx 25\%$, while lower surface density clouds become increasingly atomic-dominated.

2.2.2 Variable Area Case

The expression we have just derived applies to clouds that maintain a constant cross-sectional area as they travel outward in the wind. However, [KTOM](#) also consider the possibility of clouds that expand as they travel outward, with a cloud radius that expands $\propto a^2$ (constant solid angle) or $\propto a$ (intermediate between constant solid angle and constant area). In general if the radius of a cloud varies with distance as a^p for some power p , then the column when the cloud is at distance a is $\Sigma = \bar{\Sigma}_0 e^x a^{-p}$, and therefore evolves as $d\Sigma/da = -p\Sigma/a$. If we assume that the atomic and molecular parts expand homologously, then it is clear that the evolution equation for the atomic surface density generalises to

$$\frac{d\Sigma_{\text{HI}}}{da} = \frac{\chi_0 t_0 \dot{\Sigma}_{\text{diss},0}}{a^2 U_a(x)} - p \frac{\Sigma_{\text{HI}}}{a} \quad (6)$$

and the evolution equation for the atomic fraction is

$$\frac{df_{\text{HI}}}{da} = \frac{d}{da} \left(\frac{\Sigma_{\text{HI}}}{\Sigma} \right) = \frac{\chi_0 \dot{\Sigma}_{\text{diss},0} t_0}{\bar{\Sigma}_0 e^x} \frac{a^{p-2}}{U_a(x)} \quad (7)$$

This clearly reduces to the constant area case we have derived above when $p = 0$. We can therefore express the H I fraction at some distance a for a cloud characterised by dimensionless (log) surface density x as

$$f_{\text{HI}}(a, x) = \min \left(\xi e^{-x} \int_1^a \frac{a'^{p-2}}{U_{a'}(x)} da', 1 \right), \quad (8)$$

where we define

$$\xi \equiv \frac{\chi_0 \dot{\Sigma}_{\text{diss},0} t_0}{\bar{\Sigma}_0}. \quad (9)$$

The integral appearing in [Equation 8](#) cannot be evaluated analytically for all possible wind acceleration laws as it can be for the case of constant area and a point gravitational potential, but it is straightforward to evaluate numerically. The dimensionless quantity ξ in [Equation 8](#) can be thought of as analogous to an ionisation parameter, in that it describes a ratio of the radiation flux to the baryon density, or as describing a ratio of timescales: t_0 is the characteristic time that it takes a cloud that is launched in the wind to move away from the galaxy, while $\bar{\Sigma}_0/\chi_0 \dot{\Sigma}_{\text{diss},0}$ is the characteristic timescale required to dissociate a cloud of molecular hydrogen with a surface density equal to the mean surface density of the galaxy, $\bar{\Sigma}_0$. Values of $\xi \gg 1$ correspond to galaxies where dissociation happens fast compared to motion, values $\xi \ll 1$ to cases where motion is faster.

2.3 The total and asymptotic molecular flux

The above expression applies to a single cloud with a fixed initial (log) surface density x ; we can use this to calculate the total molecular fraction for a system in which clouds at a range of column densities

are continuously being ejected from the galaxy. In the [KTOM](#) model, the PDF of surface density with respect to mass follows a log-normal form, which we reproduce here from [Equation 8](#) of [KTOM](#):

$$p_M(x) = \frac{1}{\sqrt{2\pi\sigma_x^2}} \exp \left[-\frac{(x - \sigma_x^2/2)^2}{2\sigma_x^2} \right], \quad (10)$$

where here σ_x is the dispersion of the log-normal, which depends on the Mach number \mathcal{M} of the turbulence in the galaxy. Clouds are ejected only for $x < x_{\text{crit}}$.

Given this distribution, the total wind mass flux carried by clouds with initial column densities in the rate x to $x+dx$ is $d\dot{M} \propto p_M(x) dx$, and the atomic mass flux is $d\dot{M}_{\text{HI}} \propto f_{\text{HI}}(a, x) p_M(x) dx$, where f_{HI} is given by [Equation 8](#). We are therefore now in a position to write down the flux-averaged atomic fraction in the wind as

$$\mathcal{F}_{\text{HI}}(a) = \frac{\int_{-\infty}^{x_{\text{crit}}} f_{\text{HI}}(a, x) p_M(x) dx}{\int_{-\infty}^{x_{\text{crit}}} p_M(x) dx}. \quad (11)$$

We define $\mathcal{F}_{\text{HI}} \equiv \lim_{a \rightarrow \infty} \mathcal{F}_{\text{HI}}(a)$ as the asymptotic atomic flux, i.e., the fraction of the flux that reaches infinity in the form of atomic hydrogen; conversely, $\mathcal{F}_{\text{H}_2} = 1 - \mathcal{F}_{\text{HI}}$ is the fraction that reaches infinity in molecular form.

The dot-dashed magenta line in the bottom panel of [Figure 2](#) shows $\mathcal{F}_{\text{HI}}(a)$ estimated for same values of Γ and ξ mentioned in [Section 2.2.1](#), and using a Mach number $\mathcal{M} = 1000$, a choice that we will justify below. Even though there are individual clouds that may be entirely atomic at large a , the flux-averaged fraction of atomic gas is ~ 0.3 . Following the trends in $U_a(x)$ and f_{HI} , $\mathcal{F}_{\text{HI}}(a)$ flattens out beyond $a \sim \text{few}$, approaching its asymptotic value \mathcal{F}_{HI} .

It is worth noting that these are the *flux*-averaged atomic and molecular fractions, rather than the *mass*-averaged fractions at a given radius. The density of material at a given radius is proportional to the flux divided by the velocity, so the *mass*-averaged H I fraction is given by

$$\mathcal{F}_{\text{HI, mass}}(a) = \frac{\int_{-\infty}^{x_{\text{crit}}} f_{\text{HI}}(a, x) p_M(x) / U_a(x) dx}{\int_{-\infty}^{x_{\text{crit}}} p_M(x) / U_a(x) dx}. \quad (12)$$

However, in practice this definition differs from the flux-averaged one only in marginal cases. For this reason we will for the rest of this paper focus exclusively on flux-averaged mass fractions as defined by [Equation 11](#).

3 RESULTS

The atomic and molecular fractions in the model we have just described are fully determined by our model for cloud expansion (i.e., clouds of constant area versus constant solid angle), the gravitational potential, and three dimensionless numbers: the Eddington ratio Γ , the Mach number \mathcal{M} of the galaxy from which the wind is driven, and the ionisation parameter-like quantity ξ . In [Section 3.1](#) we seek to understand how the dimensionless numbers affect the molecular fraction in winds for a fiducial choice of cloud area and potential shape, and in [Section 3.2](#) we apply what we have learned to samples of observed galaxies.

3.1 Which parameters determine the phase balance?

We are now in a position to determine how the dimensionless numbers we have identified affect the outflow chemical state. We begin this discussion with the parameters Γ and \mathcal{M} ; [Figure 3](#) shows how

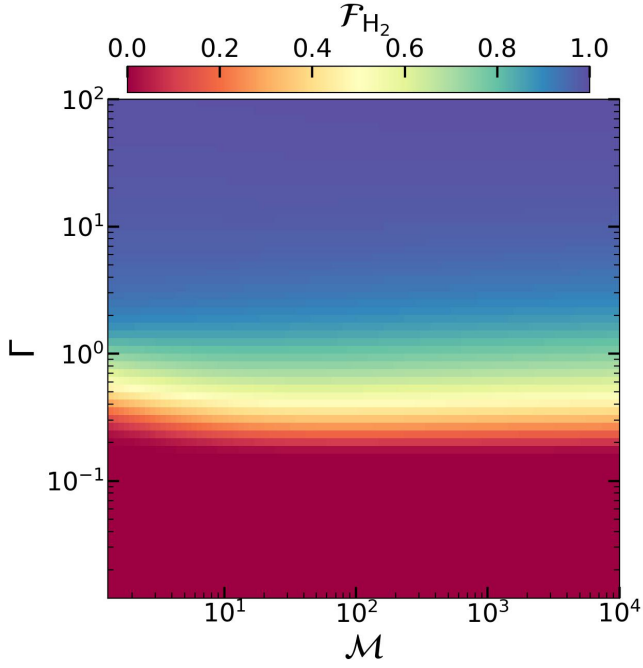


Figure 3. Flux-averaged asymptotic molecular fraction (Equation 11) as a function of Γ and \mathcal{M} for fixed $\xi = 0.0406$ and clouds of fixed area in a point potential. We see that \mathcal{F}_{H_2} is nearly independent of \mathcal{M} for $\mathcal{M} \gtrsim 10$, indicating it is not an important parameter determining how molecular the outflows are.

\mathcal{F}_{H_2} varies with these parameters at fixed $\xi = 0.0406$ and for the case of constant area clouds in a point potential; we choose these example parameters based on the analysis of the wind of M82 by Yuan et al. (2023), who find that the H I and CO outflows are best described as fixed area, point potential, and where the value of ξ comes from using their preferred galaxy parameters together with a gas surface density taken from Kennicutt (1998) in the formalism we describe below in Section 3.2. However, the qualitative results are similar for any other parameter choice. In particular, we see that the asymptotic molecular fraction is nearly independent of the Mach number in the disc once $\mathcal{M} \gtrsim 10$, a condition that will be satisfied with respect to molecular gas in almost any galaxy. The physical origin of this behaviour is easy to understand if we examine Figure 2: at large \mathcal{M} , the column density PDF in the disc becomes very broad, so that a majority of the mass flux is carried by clouds with $x \ll x_{\text{crit}}$ (redder colours in Figure 2). For these clouds gravity is unimportant ($\Gamma e^{-x} \gg 1$ in Equation 2), and they quickly accelerate to a terminal velocity that is inversely proportional to their surface density. This means that the time they spend near the galaxy being exposed to strong dissociating radiation is directly proportional to their surface density – but the amount of time required to fully dissociate a cloud is also linearly proportional to its surface density, and so this results in a molecular fraction that becomes independent of x for $x \ll x_{\text{crit}}$. This explains the behaviour shown in Figure 3: once \mathcal{M} is large enough that most flux is carried by clouds with $x \ll x_{\text{crit}}$, further increases in \mathcal{M} have no more effect on \mathcal{F}_{H_2} . We may therefore discard \mathcal{M} as an important parameter, and simply adopt the $\mathcal{M} \gg 1$ limit; for subsequent numerical results, we therefore set $\mathcal{M} = 1000$.

Having discarded \mathcal{M} , we now turn to the two remaining parameters Γ and ξ . We examine these two in Figure 4; the colourmap in each panel is identical to the one shown in Figure 3 except that instead of \mathcal{M} on the horizontal axis we have ξ . The three panels show different

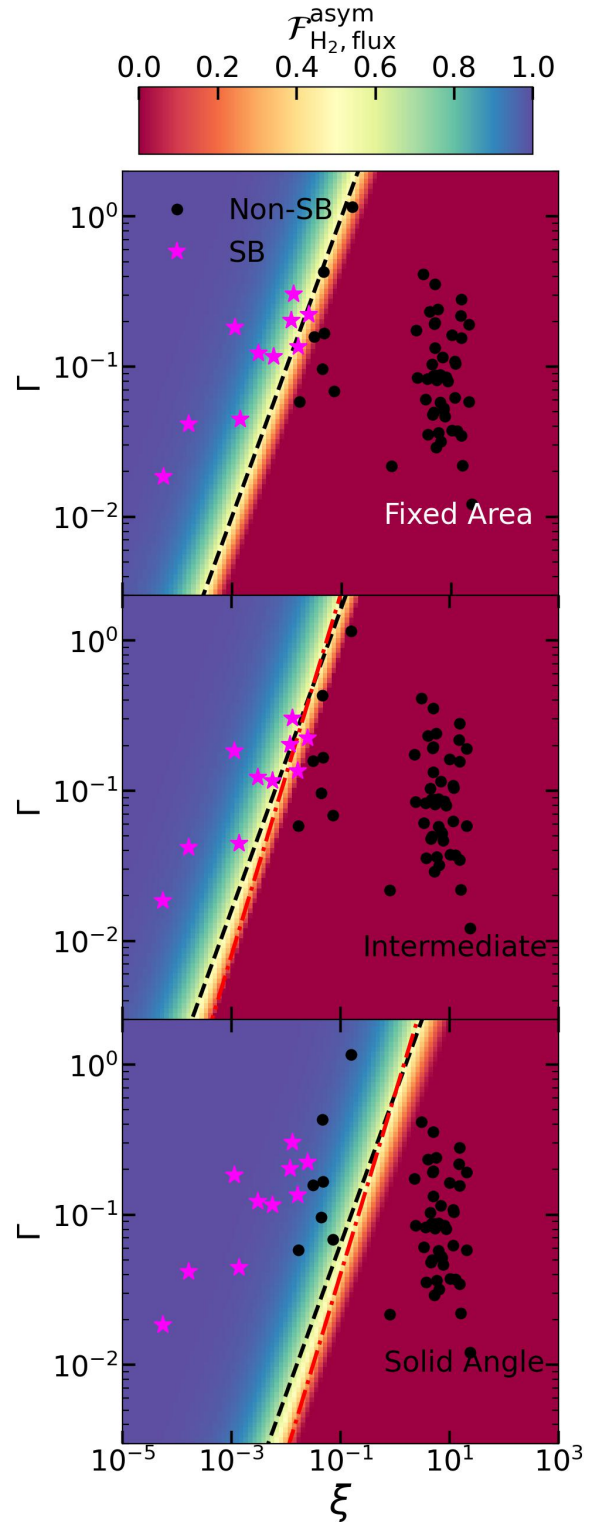


Figure 4. Same as Figure 3 except now we show the dissociation parameter ξ on the horizontal axis. The different panels show different expansion laws – fixed area (top), intermediate (middle) and constant solid angle (bottom). Black and magenta data points show the parameters of observed starburst and non-starburst galaxies, respectively; see Section 3.2 for details. Dashed and dot-dashed lines indicates a rough by-eye fit to the locus $\mathcal{F}_{\text{H}_2} = 0.5$ for point potentials (black dashed) and isothermal potentials (red dot-dashed). Note that there is no line for fixed area clouds in an isothermal potential, since that case does not generate a wind that escapes.

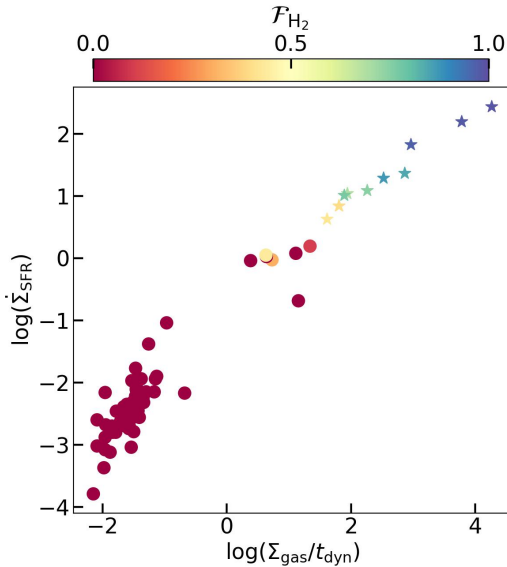


Figure 5. Star formation rate per unit area versus gas surface density per dynamical time for observed galaxies. Points are coloured by estimated outflow \mathcal{F}_{H_2} ; circles show normal galaxies, stars show starbursts. See Section 3.2 for details on the data.

expansion laws – fixed area (top), intermediate (middle) and the constant solid angle case (bottom). Evidently, the interplay between Γ and ξ is the key in determining winds’ molecular content. There is clear-cut separation between parts of parameter space where they are predominantly atomic and those where they are predominantly molecular, with the latter occupying the low ξ , high Γ corner of parameter space. The dashed black lines in each panel show rough by-eye fits to the line separating the two regimes, which follow the functional form $\log \Gamma = k \log \xi + \text{const}$ with slope $k = 1$. Intuitively, galaxies to the right and below this line have stronger radiation fields and clouds that accelerate more slowly, meaning that the clouds spend a longer time in the presence of a radiation field, resulting in purely atomic outflows. Galaxies on the other side of the line have short dynamical times and rapidly-accelerating clouds, which propels clouds away from this radiation field faster, thereby preserving a high molecular fraction.

Comparing the three panels, we see that as cloud expansion becomes more rapid, the flow becomes increasingly molecular and the black dashed lines move right, albeit by a relatively small amount. The physical origin of this effect is that, even though expansion makes clouds bigger targets for dissociating photons and thus increases their dissociation rate, it also allows them to absorb momentum from the outflow more quickly and thus escape from the region of strong dissociation faster; the latter effect proves to be (slightly) more important. By contrast, the shape of the potential has minimal effects. The red dot-dashed lines in Figure 4 are identical to the black dashed ones, except for the case of an isothermal rather than a point-mass potential, and are clearly nearly the same. Potential shape is unimportant because it matters most once clouds have travelled some distance from the central galaxy, and by the time clouds get that far, per Figure 2, their chemical state is already set.

3.2 Application to observed galaxies

Using the formalism described in Section 2, we can make predictions about the molecular/atomic fractions in outflows from observed

galaxies. To do so, however, we require a method to estimate the dimensionless parameters Γ and ξ from observables. First consider the generalised Eddington ratio, which is related to galaxy properties as (Thompson & Krumholz 2016; Krumholz et al. 2017)

$$\Gamma = \frac{\dot{p}}{4\pi GM_0 \bar{\Sigma}_0}, \quad (13)$$

where \dot{p} is the rate of momentum injection into the wind over all 4π sr and M_0 and $\bar{\Sigma}_0$ are the gravitating mass and gas surface density interior to the wind launch radius r_0 . Since M_0 is not directly observable, we rewrite it in terms of the orbital period, which is. Specifically, the orbital speed is $v_{\text{orb}} = \sqrt{GM_0/r_0}$ and the orbital period is $t_{\text{orb}} = 2\pi r_0/v_{\text{orb}}$, and thus we have $M_0 = 4\pi^2 r_0^3/Gt_{\text{orb}}$. Similarly, the momentum injection is not known, but for a supernova-driven wind we can estimate that the terminal momentum available per unit mass of stars formed after cooling losses and neglecting any enhancement due to clustering is $\langle p_*/m_* \rangle \approx 3000 \text{ km s}^{-1}$ (e.g., Martizzi et al. 2015; Kim et al. 2017; Gentry et al. 2019). Thus we can write $\dot{p} = \pi r_0^2 \dot{\Sigma}_* \langle p_*/m_* \rangle$, where $\dot{\Sigma}_*$ is the star formation rate per unit area. Inserting these expressions into Equation 13 gives

$$\Gamma = \frac{\dot{\Sigma}_* t_{\text{orb}}^2}{16\pi^2 r_0 \bar{\Sigma}_0}. \quad (14)$$

The right hand side now depends only on the surface densities of gas and star formation, the size of the galaxy, and the orbital period, all quantities that are directly observable. Similarly, for the dissociation parameter ξ (Equation 9), we take $t_0 = r_0/v_0 = t_{\text{orb}}/2^{3/2}\pi$. The most uncertain parameter is χ_0 , the dissociating photon flux in the galaxy; this could be either higher or lower than in the Milky Way for more intensely star-forming galaxies – higher because the photon injection rate is higher due to more intense star formation, lower because there is also more gas and thus more extinction. We will adopt $\chi_0 = 1$ out of ignorance, and discuss the implications of this uncertainty below. Given these approximations, we have

$$\xi = \frac{\dot{\Sigma}_{\text{diss},0} t_{\text{orb}}}{2^{3/2}\pi \bar{\Sigma}_0}, \quad (15)$$

and again all quantities on the right hand side are now direct observables.

We take measurements of $\bar{\Sigma}_0$, $\dot{\Sigma}_*$, r_0 , and t_{orb} from a subset of the galaxy sample compiled by Krumholz et al. (2012), drawn in turn from Kennicutt (1998), Daddi et al. (2010), and Genzel et al. (2010). We take $\dot{\Sigma}_*$ and $\bar{\Sigma}_0$ directly from Krumholz et al.’s tables; these have been standardised to use a common initial mass function and model for α_{CO} . For the galaxies in Krumholz et al.’s compilation that originally come from Daddi et al., we take radii and orbital periods from Daddi et al.’s tables. For those that come from Genzel et al., we take r_0 from their reported half-light radii, and we set $t_{\text{orb}} = 2\pi r_0/v_d$, where v_d is their reported maximum circular velocity. Finally, for the subset of the Krumholz et al. compilation drawn from Kennicutt, we use Kennicutt’s reported orbital periods, and we derive radii from the angular sizes reported in Kennicutt (1989) together with distances from SIMBAD (Wenger et al. 2000).

We show the location of this galaxy sample in the (Γ, ξ) plane in Figure 4; points are colour-coded by whether Krumholz et al. (2012) classify each galaxy as a starburst or a non-starburst. We also show the data on the traditional Kennicutt-Schmidt plot colour-coded by derived \mathcal{F}_{H_2} (assuming constant area clouds) in Figure 5. The clear conclusion from these figures is that there is a transition from atomic-dominated outflows in non-starburst galaxies to molecular-dominated outflows in strong starbursts, with weak circumnuclear and dwarf starbursts (e.g., M82) and high-redshift giant

star-forming discs straddling the boundary. Near this boundary the molecular fraction depends on cloud expansion law and on the poorly known dissociating radiation flux χ_0 (to which ξ is proportional), but most galaxies lie far enough from the boundary that neither of these uncertainties plausibly change the result. We note that our finding that outflows in galaxies like the Milky Way should completely dissociate by the time they reach distances of a few r_0 , while those in weak starburst galaxies like M82 should retain a substantial molecular component to distances much larger than r_0 , is in fact consistent with what is observed in those galaxies (Milky Way: Di Teodoro et al. 2020; Noon et al. 2023; M82: Leroy et al. 2015; Yuan et al. 2023). We can further note that the starburst and non-starburst samples have fairly similar values of Γ – the higher momentum injection in the starbursts is largely balanced by their higher star formation rates – and differ primarily in their values of ξ . This is driven in turn by the fact that starbursts have both high gas surface density and short dynamical times compared to normal galaxies.

4 DISCUSSION AND CONCLUSION

We present an analytic model to describe the molecular content of galactic winds. We first show that, unlike the balance between ionised and neutral material in winds, the balance between neutral and molecular hydrogen is almost certainly controlled by radiative rather than collisional processes, and thus the presence of molecules in winds that contain any amount of neutral material is determined by the galactic photon field. As a result, the molecular fraction is determined primarily by two dimensionless parameters: an ionisation parameter-like quantity ξ that describes the ratio of the dissociation and dynamical times in the galaxy, and a generalised Eddington ratio Γ that controls how quickly clouds in the wind are accelerated away from the disc and its dissociating radiation field. By contrast, other parameters such as the density distribution in the wind-launching galaxy (as parameterised in our model by the turbulent Mach number), the shape of the galactic potential, and the rate at which clouds that are swept into the wind expand all have only marginal effects.

Applying this model to a sample of observed galaxies, we predict a dichotomy between starbursts and normal star-forming galaxies, with the non-starbursts having predominantly atomic composition in the neutral wind phase and the starbursts predominantly molecular. The difference arises because starburst have both higher gas surface densities and shorter dynamical times than normal star-forming galaxies; the former factor means that dissociating radiation requires longer to eat through the molecular material, while the latter factor means that outflows escape quickly and thus there is less time available for the radiation to do so.

Our predictions should be testable by future campaigns studying galactic outflows. In particular, as a new generation of H I facilities that will be much more sensitive to low surface-brightness extended emission (e.g., MeerKAT, ASKAP, and eventually the full SKA) come online, it should be possible to identify a much larger number of atomic-dominated outflows than the handful currently known. Our model predicts that such outflows should be common for normal star-forming galaxies, but should decline in importance relative to molecular outflows as we move to the strong starburst regime. In particular, we predict that strong starbursts like Arp 220 should have substantial molecular outflows, but that these outflows should comparatively poor in atomic hydrogen.

ACKNOWLEDGEMENTS

AV and MRK acknowledge support from the Australian Research Council through awards FL220100020 and DP230101055. The authors thank J. Chisholm and D. Fisher for helpful conversations.

DATA AVAILABILITY

No new data were obtained as part of this work.

REFERENCES

- Bolatto A. D., et al., 2013, *Nature*, 499, 450
 Butsky I. S., Hummels C. B., Hopkins P. F., Quinn T. R., Werk J. K., 2024, *arXiv e-prints*, p. arXiv:2402.03419
 Chen Z., Oh S. P., 2023, *arXiv e-prints*, p. arXiv:2311.04275
 Daddi E., et al., 2010, *ApJ*, 713, 686
 Di Teodoro E. M., McClure-Griffiths N. M., Lockman F. J., Denbo S. R., Endsley R., Ford H. A., Harrington K., 2018, *ApJ*, 855, 33
 Di Teodoro E. M., McClure-Griffiths N. M., Lockman F. J., Armillotta L., 2020, *Nature*, 584, 364
 Draine B. T., 1978, *ApJS*, 36, 595
 Fielding D. B., Bryan G. L., 2022, *ApJ*, 924, 82
 Gentry E. S., Krumholz M. R., Madau P., Lupi A., 2019, *MNRAS*, 483, 3647
 Genzel R., et al., 2010, *MNRAS*, 407, 2091
 Ginolfi M., et al., 2017, *MNRAS*, 468, 3468
 Glover S. C. O., Mac Low M.-M., 2007, *ApJS*, 169, 239
 Gong M., Ostriker E. C., Wolfire M. G., 2017, *ApJ*, 843, 38
 Huang S., Katz N., Davé R., Oppenheimer B. D., Weinberg D. H., Fardal M., Kollmeier J. A., Peebles M. S., 2020, *MNRAS*, 493, 1
 Huang S., Katz N., Cottle J., Scannapieco E., Davé R., Weinberg D. H., 2022, *MNRAS*, 509, 6091
 Indriolo N., McCall B. J., 2012, *ApJ*, 745, 91
 Kennicutt Robert C. J., 1989, *ApJ*, 344, 685
 Kennicutt Robert C. J., 1998, *ApJ*, 498, 541
 Kim C.-G., Ostriker E. C., Raileanu R., 2017, *ApJ*, 834, 25
 Kim C.-G., et al., 2020a, *ApJ*, 900, 61
 Kim C.-G., et al., 2020b, *ApJ*, 903, L34
 Krumholz M. R., 2014, *MNRAS*, 437, 1662
 Krumholz M. R., McKee C. F., Tumlinson J., 2009, *ApJ*, 693, 216
 Krumholz M. R., Dekel A., McKee C. F., 2012, *ApJ*, 745, 69
 Krumholz M. R., Thompson T. A., Ostriker E. C., Martin C. L., 2017, *MNRAS*, 471, 4061
 Leroy A. K., et al., 2015, *ApJ*, 814, 83
 Li M., Bryan G. L., 2020, *ApJ*, 890, L30
 Martini P., Leroy A. K., Mangum J. G., Bolatto A., Keating K. M., Sandstrom K., Walter F., 2018, *ApJ*, 856, 61
 Martizzi D., Faucher-Giguère C.-A., Quataert E., 2015, *MNRAS*, 450, 504
 Noon K. A., Krumholz M. R., Di Teodoro E. M., McClure-Griffiths N. M., Lockman F. J., Armillotta L., 2023, *MNRAS*, 524, 1258
 Raskutti S., Ostriker E. C., Skinner M. A., 2017, *ApJ*, 850, 112
 Rathjen T.-E., et al., 2021, *MNRAS*, 504, 1039
 Schneider E. E., Ostriker E. C., Robertson B. E., Thompson T. A., 2020, *ApJ*, 895, 43
 Smith M. C., et al., 2024, *MNRAS*, 527, 1216
 Sternberg A., Le Petit F., Roueff E., Le Bourlot J., 2014, *ApJ*, 790, 10
 Tacconi L. J., Genzel R., Sternberg A., 2020, *ARA&A*, 58, 157
 Tchernyshyov K., 2022, *ApJ*, 931, 78
 Thompson T. A., Krumholz M. R., 2016, *MNRAS*, 455, 334
 Veilleux S., Maiolino R., Bolatto A. D., Aalto S., 2020, *A&ARv*, 28, 2
 Vijayan A., Krumholz M. R., Wikbing B. D., 2024, *MNRAS*, 527, 10095
 Walter F., et al., 2017, *ApJ*, 835, 265
 Weinberger R., Hernquist L., 2023, *MNRAS*, 519, 3011
 Wenger M., et al., 2000, *A&AS*, 143, 9
 Yuan Y., Krumholz M. R., Martin C. L., 2023, *MNRAS*, 518, 4084

This paper has been typeset from a \TeX/L\AA\TeX file prepared by the author.